JOURNAL OF PROPULSION AND POWER
Vol. 17, No. 5, September–October 2001

Development of Thermal Barriers for Solid Rocket Motor Nozzle Joints

Bruce M. Steinetz* and Patrick H. Dunlap, Jr.†
NASA John H. Glenn Research Center at Lewis Field, Cleveland, Ohio 44135

Space shuttle solid rocket motor case assembly joints are sealed using conventional O-ring seals that are protected from 5500+°F combustion gases by thick layers of insulation and special joint-fill compounds. In the current nozzle-to-case joint design NASA has observed hot gas penetration through defects in the joint-fill compound to the innermost O-ring in one out of seven motors. While not threatening motor safety, evidence of hot gas penetration to the O-rings results in extensive reviews before resuming flight. This paper presents burn-resistance, temperature drop, flow, and resiliency test results for several types of NASA braided carbon fiber thermal barriers that are being implemented in a redesign of the nozzle-to-case joint. In burn-resistance tests the thermal barriers lasted for over six minutes when exposed to the flame of an oxyacetylene torch at 5500°F. Temperature drops of 2500 to 2800°F were measured through the diameter of the thermal barrier in a compressed state when subjected to an oxyacetylene torch flame. Gas temperatures $\frac{1}{4}$ in. downstream of the thermal barrier were within the downstream O-ring temperature limit of 600°F. In subscale rocket "char" motor tests the thermal barrier reduced the incoming 3200°F hot gas by 2200°F, spread the incoming jet flow, and blocked hot slag, thereby protecting the downstream O-rings.

Introduction

THE need for high temperature (1500 to 2000°F) compliant seals in advanced gas turbine engine designs led to the development of rope seals braided out of newly developed ceramic fibers and superalloy wires. Previous seal research yielded several braided rope seal designs that demonstrated the ability to both seal and serve as compliant mounts under aggressive temperature and pressure requirements.[1,2] However, Steinetz and Dunlap[3] showed that these seals do not last for more than a few seconds when subjected to the extremely hot 5500+°F combustion gases that are found in the space shuttle solid rocket motor. Thus, other materials were considered to evolve the braided rope seal design into a thermal barrier for use at extreme transient temperatures.

The space shuttle reusable solid rocket motor (RSRM) assembly joints are sealed using conventional O-ring seals. The 5500+°F combustion gases are kept a safe distance away from the seals by thick layers of phenolic or rubber insulation. Special joint-fill compounds are used to fill the joints in the insulation to prevent a direct flowpath to the seals. Normally, these two stages of protection are enough to prevent a direct flowpath of the 900-psi (1 psi = 6894 Pa or N/m^2) hot gases from reaching the seals. Occasionally, seals have experienced charring caused by parasitic leakage paths that open up in the joint-fill compounds during rocket operation. Inspection during disassembly of space shuttle solid-rocket-motor nozzle joints from RSRM-44 and RSRM-45 revealed O-ring erosion of joint 3 primary O-ring seals[4] (Fig. 1). Subsequent improvements in joint-fill compound application techniques have apparently overcome the joint 3 charring problem. However, a number of nozzle joints including the nozzle-to-case joint and joint 2 continue to show hot gas penetration through the joint-fill compound. The current nozzle-to-case joint design incorporates primary, secondary, and wiper (innermost) O-rings and polysulfide joint-fill compound. In the current design one out of seven motors experiences hot gas to the wiper O-ring. Though the condition does not threaten motor safety, evidence of hot gas to the wiper O-ring results in extensive reviews before resuming flight. NASA and solid-rocket-motor manufacturer Thiokol are examining a redesign of the nozzle-to-case joint in which a more reliable J-leg design and a thermal barrier are implemented, and the joint-fill compound is eliminated (Fig. 1). The J-leg is molded into the insulation and contacts the mating surface of the adjoining element. Rocket pressurization acts to further preload the J-leg increasing its effectiveness. The basic J-leg design has been applied successfully to fixing the field joints in the redesign effort following the space shuttle accident.[5] While compressed between the J-leg and adjoining element, the thermal barrier is intended to resist any hot gases the J-leg does not block and prevent them from reaching the wiper O-ring. The braided carbon thermal barrier being developed at NASA John H. Glenn Reserch Center is the leading candidate based on the results presented herein.

The thermal barrier for the shuttle solid rocket motor has unique requirements, including the following, among others:

1) Sustain extreme temperatures (2500 to 5500°F) during solid-rocket-motor burn (2 min and 4 s.) without loss of integrity.

2) Drop incoming gas temperatures (up to 3200°F) in the joint to levels acceptable to fluorocarbon O-rings (≤600°F, short term) to prevent O-ring damage, including char and erosion.

3) Exhibit some permeability to permit the joint cavity (between thermal barrier and O-ring) to reach chamber pressure (900 psi) in acceptable time.

4) Exhibit adequate resiliency/springback to accommodate limited joint movement and manufacturing tolerances in these large (8.5-ft-diam) nozzle segments (1 ft = 0.3048 m).

5) Diffuse/spread incoming narrow (0.08-in-diam) hot gas jets to reduce their damaging effects on the downstream O-rings.

6) Block hot slag (i.e., molten alumina, etc.) entrained in the gas stream from reaching the O-rings.

Steinetz and Dunlap[3] performed a number of tests on 0.125- and 0.200-in.-diam braided carbon fiber thermal barriers demonstrating that they met the burn-resistance, permeability, and resiliency criteria.

The main objective of the current study is to fully characterize two braided carbon fiber thermal barrier designs (denoted Carbon-3 and Carbon-6) by assessing their transient thermal response when subjected to a high-temperature torch and by characterizing their permeability, resiliency, and burn resistance. The Carbon-6 design is currently being tested by both NASA and Thiokol for the nozzle-to-case

Received 31 January 2000; presented as Paper 99-2823 at the AIAA/ASME/SAE/ASEE 35th Joint Propulsion Conference and Exhibit; Los Angeles, CA, 22–25 June, 2000; revision received 1 February 2001; accepted for publication 26 February 2001.

*Senior Research Engineer, Mechanical Components Branch. Member AIAA.

†Mechanical Engineer, Mechanical Components Branch. Member AIAA.

Table 1 Thermal barrier construction matrix

Barrier type	Size diameter, in.	Core: Material	Core: Denier	Core: Fiber diameter, in.[a]	Core: Number of yarns	Sheath: Material	Sheath: Denier	Sheath: Fiber diameter, in.[a]	Sheath: Number of layers	Sheath: Number carriers per layer	Sheath: Number of yarns per bundle	Sheath: Braid angle, deg
						Carbon						
Carbon-1	0.114	Grafil[b]				Thornel[c]						
		34–700 12K	7200	2.76×10^{-4}	4	T-300 1K	600	2.8×10^{-4}	5	8	1	45
Carbon-2	0.125	Grafil				Thornel						
		34–700 12K	7200	2.76×10^{-4}	1	T-300 1K	600	2.8×10^{-4}	10	8	1	45
		34–700 3K	1800		1							
Carbon-2A	0.125	Grafil				Thornel						
		34–700 12K	7200	2.76×10^{-4}	1	T-300 1K	600	2.8×10^{-4}	9	8	1	45
		34–700 3K	1800		1							
Carbon-3	0.200	Grafil				Thornel				12 in 1–2		65 in 1st
		34–700 12K	7200	2.76×10^{-4}	10	T-300 1K	600	2.8×10^{-4}	5	24 in 3–5	1	60 in 5th
Carbon-4	0.194	Amoco[d]				Thornel				12 in 1–2		65 in 1st
		P25 2K	2900	4.4×10^{-4}	21	T-300 1K	600	2.8×10^{-4}	5	24 in 3–5	1	60 in 5th
Carbon-6	0.260	Grafil				Thornel				8 in 1–5		17 in 1st
		34–700 12K	7200	2.76×10^{-4}	1	T-300 1K	600	2.8×10^{-4}	10	12 in 6–7	1	45 in 2–10
						T-300 3K	1800			16 in 8–10		
						All-ceramic						
NTWAC-2	0.120	NX 550[e]	700	3.2×10^{-4}	109	NX 550	700	3.2×10^{-4}	2	8	1	56

[a] 1×10^{-3} in. = 25 μm.
[b] Grafil type 34-700 Carbon fibers, Grafil Inc. product. 12K-12,000 fiber ends.
[c] Thornel T-300 carbon fibers, Amoco Performance Products, Inc. product.
[d] Amoco P25 pitch fibers, Amoco Performance Products, Inc. product.
[e] NX 550 = Nextel 550 fiber, 3M product, 73% Al_2O_3, 27% SiO_2.

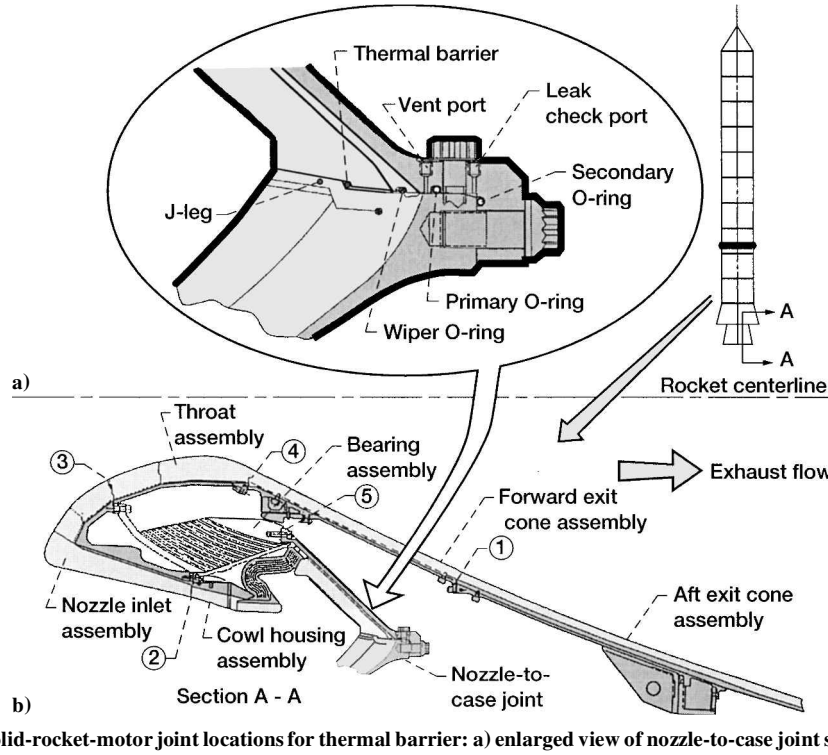

Fig. 1 Potential shuttle solid-rocket-motor joint locations for thermal barrier: a) enlarged view of nozzle-to-case joint showing J-leg, wiper, primary, and secondary O-rings, leak-check port, and proposed thermal barrier location and b) overall nozzle cross section (half-view).

joints of the shuttle solid rocket motor. Subscale rocket char motor tests were performed to assess the thermal barrier's (Carbon-6) thermal response and heat resistance under actual rocket conditions.

Test Apparatus and Procedures

Thermal Barrier Specimens

Carbon-3 and Carbon-6 were subjected to burn, temperature drop, flow, and compression tests. Carbon-6 was also tested in a subscale char motor. Limited testing was performed on the Carbon-4 design. Table 1 summarizes the relevant architecture parameters for the thermal barrier designs that were tested.

All thermal barriers were composed of a uniaxial core of fibers overbraided with various numbers of sheath layers. The Carbon-6 design had 10 sheath layers and a 0.26-in. diam. Carbon-6 had good flexibility and compliance properties because it was braided with a more open architecture. The Carbon-3 design had a 0.20-in. diam and was made with a large degree of uniaxial core fibers overbraided with five sheath layers. Carbon-3 was a tight braid that was not as flexible as Carbon-6. Carbon-4 had 4.4×10^{-4} in. (11-μm)

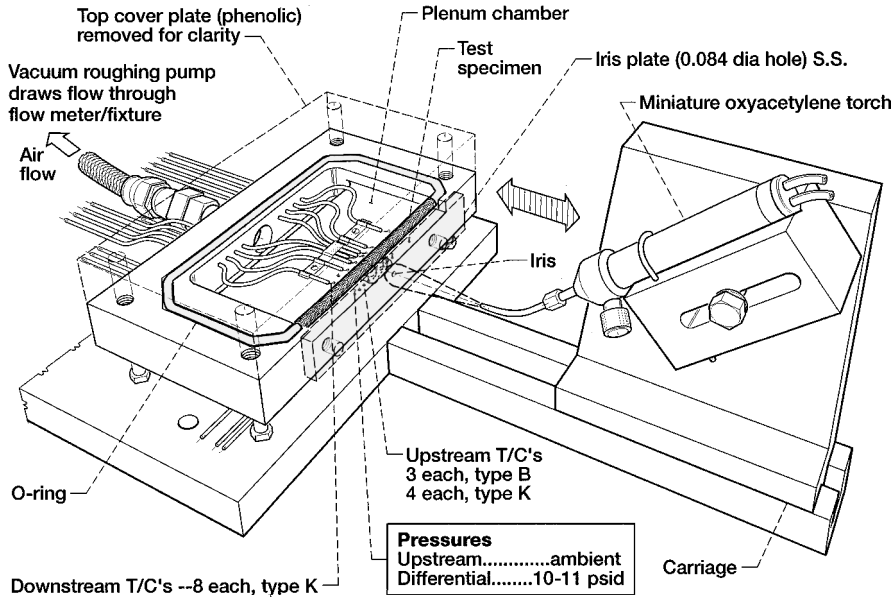

Fig. 2 Schematic of temperature drop test fixture.

pitch-based Amoco P25 fibers in its core to evaluate core fiber diameter effects on performance, while the core fibers of all of the other carbon thermal barriers were 2.76×10^{-4} in. (6.9-μm) PAN-based Grafil type 34-700 fibers. PAN-based Thornel T-300 carbon fibers with a 2.8×10^{-4} in. (7-μm) diam were used in the sheaths of all of the thermal barrier designs.

Thermal Barrier Porosity Measurements

To assess thermal barrier porosity while under compression, samples of the Carbon-3 and Carbon-6 designs were examined in a compressed state using a photographic stereomicroscope. Four $\frac{1}{2}$-in. long specimens of both types of thermal barriers were prepared and weighed using a precision electronic balance. The exact length of each specimen was measured using vernier calipers. Each specimen was then clamped between two steel plates and subjected to a 20% compression. While the specimens were compressed, a light layer of cyanoacrylic glue was applied to the surface of each specimen so that they would maintain their compressed shape upon removal from the fixture.

Four specimens were examined for both Carbon-3 and Carbon-6. Both ends of each specimen were examined and photographed at 10× in the microscope so that eight cross-section photos were examined for both thermal barrier designs. Each cross-section assumed an ellipsoidal shape in its compressed state. The dimensions of each ellipse were measured using vernier calipers. These dimensions were then used to calculate the cross-sectional area of both ends of each specimen. An average cross-sectional area was calculated for each specimen and multiplied by the specimen length to determine the specimen volume. Specimen density was then calculated by dividing the weight of the specimen by its volume. An average density at 20% compression was found for both Carbon-3 and Carbon-6 by averaging the densities of the four specimens of each design. The porosity of each thermal barrier design at 20% compression was calculated using the following relationship:

$$\text{Porosity} = 1 - (\rho_{\text{ThermalBarrier}} / \rho_{\text{CarbonFiber}})$$

In this relationship the density of each thermal barrier design was divided by the density of an individual carbon fiber (0.064 lb/in.^{3}) (1 lbm/in^3 = 27680 kg/m^3). Thus, a thermal barrier design would have a porosity of zero if it had no gaps and assumed the density of an individual fiber.

Burn Tests

A screening test was developed to evaluate thermal barrier burn resistance under simulated rocket motor combustion temperatures (5500°F) by aiming a "neutral" flame[6] of an oxyacetylene-welding torch at the center section of a 4-in. thermal barrier specimen. In these tests the amount of time required to completely cut through the specimen was measured. Time for cutthrough was measured from the instant the flame touched the specimen until the specimen was completely cut into two separate pieces. A detailed description and an illustration of the fixture used to perform these tests can be found in the paper by Steinetz and Dunlap.[3]

Temperature Drop Tests

A test fixture was developed to measure the temperature drop across and along the thermal barriers in a compressed state when subjected to the neutral flame of an oxyacetylene torch simulating rocket temperatures (Fig. 2). Flow was drawn through the thermal barrier using a vacuum roughing pump to lower pressure on the downstream side of the thermal barrier while leaving the upstream side at ambient conditions. Flow through the thermal barrier was measured using a flow meter positioned between the fixture and the roughing pump. The volume downstream of the thermal barrier was an enclosed plenum chamber sealed by an O-ring between the bottom plate and a top plate. The thermal barrier was compressed at 20% linear compression. Other compressions are possible by placing shims under the thermal barrier. The fixture was made out of phenolic insulation having low thermal conductivity that simulates the solid-rocket-motor insulating material and minimizes parasitic heat loss.

The torch flame was applied to the thermal barrier to simulate a leak path of hot gases through the nozzle joint. The flame with temperatures up to 3200°F was positioned on a small area of the thermal barrier. An "iris plate" with a 0.084-in.-diam hole concentrated a "laser-like" column of flame onto the thermal barrier, simulating a hot gas jet flowing through the rocket nozzle joint. The iris plate was positioned about $\frac{1}{4}$-in. away from the specimen. The jet was directed at the center of the specimen both span- and height-wise.

To measure the surface temperature distribution along the thermal barrier span, thermocouples were placed on both the upstream (hot) and downstream (cold) sides. The thermal barrier specimen sat between these two rows of thermocouples in a 0.040-in. deep groove. The thermocouples measured how the flame spread along the thermal barrier, how much temperature drop occurred across the thermal barrier, and how heat was conducted along its length. The fixture was instrumented with seven thermocouples upstream of the thermal barrier and eight downstream thermocouples. On the upstream side the center Type B thermocouple was placed directly in line with the center of the hole in the iris plate so that it measured the

hottest flame temperature at the surface of the thermal barrier. Type B thermocouples were then positioned $\frac{1}{4}$ in. on either side of the center thermocouple (Fig. 2). The remaining four thermocouples on the hot side were Type K thermocouples, and they were placed $\frac{1}{2}$ and 1 in. on either side of the center thermocouple. Seven of the eight Type K thermocouples downstream of the thermal barrier were spaced so that they were directly in line with those upstream of the thermal barrier. The remaining Type K thermocouple was positioned $\frac{1}{4}$ in. (approximately one thermal barrier diameter) downstream of the thermal barrier in line with the center thermocouple and measured the bulk air temperature.

Thermocouple Selection

Fine gauge wire open-bead thermocouples were used to quickly and accurately measure changes in the surface temperature distribution along the thermal barrier. The time constant and response rate of a thermocouple is controlled by the size of its wires and the diameter of the junction ball that is formed between the wires. The wire diameters used for the Type B and Type K thermocouples were 0.010 and 0.0125 in., respectively. A typical thermocouple junction ball has a diameter about 50% larger than the wires in the thermocouple. Calculations of the time constants for junction balls with a diameter of 0.015 to 0.019 in. showed that these thermocouples would have a time constant of about $\frac{1}{2}$ s.

Pressure/Flow Transducers

An absolute pressure transducer measured the pressure upstream of the thermal barrier while a differential transducer measured the pressure drop across a specimen. Flow through the thermal barrier was measured using a 0 to 100 SLPM (standard liters per minute) flow meter. Data were acquired from all of this instrumentation at a sampling rate of 10 Hz using Keithley data acquisition hardware and Labtech Notebook software.

For each test a 5-in. thermal barrier specimen was prepared and installed into the groove in the fixture. The 14 thermocouples that measured the surface temperature along the specimen were slipped into the outer sheath layer of the thermal barrier and adjusted so that they were spaced properly. To prevent parasitic leakage, the plenum chamber O-ring was then positioned so that it was snug against the ends of the thermal barrier. The vacuum pump was turned on for several minutes to cause the pressure drop and to achieve a steady flow rate through the specimen before applying the torch. The oxyacetylene torch was adjusted until a neutral flame was formed. The torch was slid along a machined groove until it was properly positioned in front of the hole in the iris plate. The torch was left on the specimen for 30 or 60 s and then pulled away from the fixture and shut off. Sometimes repeat tests were performed on the same specimen to examine the effects of repeated flame exposures. Torch nozzle spacing to the iris plate proved to be important in controlling the maximum hot side temperature without melting the center Type B thermocouple (platinum-rhodium, $T_{\text{melt}} = 3308^{\circ}\text{F}$). Torch spacings for Carbon-3 and Carbon-6 were 0.265 and 0.160 in., respectively.

Flow Tests

Flow tests were performed on the thermal barriers in a high-temperature flow and durability test rig shown schematically in Fig. 3. The test rig is capable of operating at temperatures from room temperature to 1500°F, pressures between 0 and 100 psig, and flows of 0 to 3.5 SCFM (standard cubic feet per minute, conversion 1 SCFM = 28.3 SLPM). Specimen length was 7.50 ± 0.05 in., and the thermal barriers were mounted into a groove in the piston. The free ends of the specimens were joined together in the piston groove using a $\frac{1}{4}$-in. lap joint. Preload was applied to the specimens through a known interference fit between the thermal barrier and the cylinder inner diameter. To vary the amount of preload, the interference fit was modified by mounting different thicknesses of stainless-steel shims behind the specimen in the piston groove. During flow testing, hot pressurized air entered at the base of the cylinder and flowed to the test specimen that sealed the annulus created by the cylinder and piston walls (0.007-in. radial gap). The durability of the

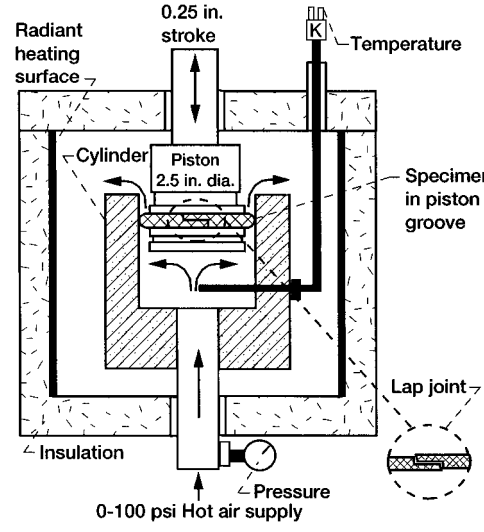

Fig. 3 Schematic of flow fixture.

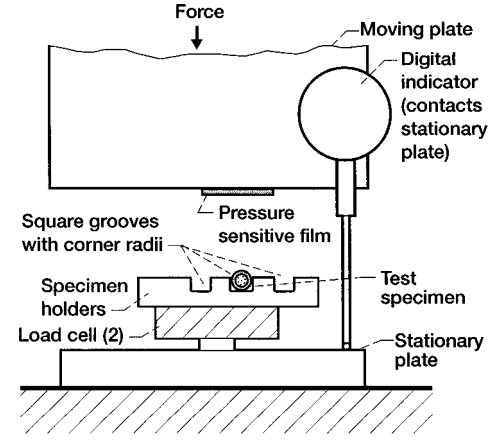

Fig. 4 Schematic of compression fixture.

thermal barriers at high temperatures was examined by subjecting them to scrub cycles in which the piston and thermal barrier were reciprocated in the cylinder.

Flow data were recorded before scrubbing at temperatures of 70 and 500°F and after scrubbing at 70, 500, and 900°F. Specimens were subjected to 10 scrub cycles at 500°F. At each temperature flow data were recorded at pressures of 2, 5, 10, 30, 60, 90, and 100 psid (or as high as could be recorded within the limits of the flow meters) with the downstream pressure at ambient pressure. Primary and repeat flow tests were performed on the Carbon-3 and Carbon-4 designs for diametral or linear compressions of 0.040 and 0.050 in. (20 and 25% linear compressions) and on the Carbon-6 design at linear compressions of 0.052 and 0.065 in. (20 and 25% linear compressions). A detailed description of the hardware and procedure used to perform these tests can be found in the papers by Steinetz et al.[1] and Steinetz and Adams.[2]

Compression Tests

Compression tests were performed to determine thermal barrier preload and resiliency behavior at room temperature using a precision linear slide compression test fixture shown schematically in Fig. 4. A 1 $\frac{1}{2}$-in.-long specimen was loaded into a stationary grooved specimen holder, and an opposing plate was compressed against the specimen. Stainless-steel shims were placed in the groove behind the specimens to vary the amount of linear compression. The amount of compressive load on the specimen was measured vs the amount of compression. Multiple load cycles were applied to the specimen before the preload data point was recorded to remove effects of the hysteresis and permanent set that accumulate with load cycling

of the specimens. Most permanent sets occurred within the first four load cycles. A pressure-sensitive film mounted on the opposing plate was used to determine the contact width of the specimen as it was compressively loaded. The footprint length (nominal 1 in.) and width at the end of the fourth load cycle were used along with the measured load vs compression data to calculate the estimated preload and residual interference corresponding to a given linear crush value.[1] Residual interference is defined as the distance the specimen will spring back while maintaining a load of at least 1 lb/in. of specimen.

Compression tests were performed on the Carbon-3 and Carbon-6 designs to determine the specimen preloads corresponding to the linear crushes used in the flow experiments. Tests were performed at compressions of 20, 25, and 30% of each specimen's overall diameter. Primary and repeat compression tests were performed. The hardware and procedure used to perform these tests are described in detail by Steinetz et al.[1]

Subscale Rocket Char Motor Tests

As part of the development process of the thermal barrier, Thiokol Corporation performed tests using a subscale (70 lbm) rocket char motor. In these tests the NASA Carbon-6 0.260-in. cross-sectional diameter thermal barrier impeded hot gas flow through an intentional circumferential defect between rocket-case insulation blocks. The thermal barrier compression was 20%. The insulation blocks were modified to accommodate a $5\frac{1}{8}$-in.-diam thermal barrier. The free ends of the specimen were joined together using a lap joint. The 0.060-in. defect was much larger than any defects that would normally form through the gap-fill material in the actual rocket nozzle joint, but this size was chosen to force gas flow through the thermal barrier under very extreme conditions. Burning solid rocket propellant, the rocket fired for 11 s and generated 900-psi pressures and 5000°F (estimated) chamber temperatures. Hot gas flowed to the thermal barrier while upstream and downstream temperatures and pressures were recorded. The char motor incorporated an outboard plenum chamber, or reservoir, to simulate the volume (80 in.^{3}) between the thermal barrier and the fluorocarbon O-ring seals. This reservoir ensured that flow would pass through the thermal barrier. The reservoir started at ambient pressure and then quickly reached chamber pressure, simulating the actual RSRM joint-fill time. After the volume between the thermal barrier and fluorocarbon O-ring pressurizes in the rocket nozzle joint, charring risk to the fluorocarbon O-ring is virtually eliminated.

Results and Discussion

Thermal Barrier Porosity Measurements

Measured values for thermal barrier density and porosity at 20% compression are presented in Table 2 for the Carbon-3 and Carbon-6 thermal barrier designs. A 20% compression level was chosen, as this is the compression level selected for the nozzle-to-case joint thermal barrier. The densities/porosities of braided structures are important for understanding their thermal and flow response characteristics.

Carbon-3 had a higher density (0.041 lb/in.^{3}) and a lower porosity (0.37) than did Carbon-6 (0.032 lb/in.^{3} and 0.50, respectively). This can be attributed to the differences in braid architecture between these two designs as shown in Table 1. Carbon-3 had a core composed of 10 uniaxial 12K yarns of Grafil 34-700 carbon fibers—a large fraction of its cross section, whereas Carbon-6 only had one 12K yarn in its core. Carbon-6 had 10 sheath layers of braided carbon fibers, whereas Carbon-3 only had five layers. Carbon-6 also had a lower sheath braid angle and fewer carriers per sheath layer to produce a softer, more flexible thermal barrier. Because the uniaxial fibers in the core pack together much better than the braided fibers that cross over each other in the sheath, the Carbon-3 design with a greater percentage of core fibers is naturally more dense and less porous. Steinetz and Dunlap[3] showed previously that the density of a braided carbon thermal barrier was inversely related to the number of sheath layers.

Burn Test Results

The amount of time to burn through each type of thermal barrier is shown in Fig. 5. In this figure the number of specimens that were tested is given next to the name of each thermal barrier type, and the average burn-through time is found above each bar. As shown previously by Steinetz and Dunlap,[3] carbon fiber thermal barriers

Table 2 Measured thermal barrier porosity at 20% compression

Thermal barrier type	Number of sheath layers	Diameter in.	Thermal barrier density, lb/in.^{3}	Carbon fiber density, lb/in.^{3}	Porosity[a]
Carbon-3	5	0.200	0.041	0.064	0.37
Carbon-6	10	0.260	0.032	0.064	0.50

[a] Porosity $= 1 - \rho_{TB}/\rho_{CF}$.

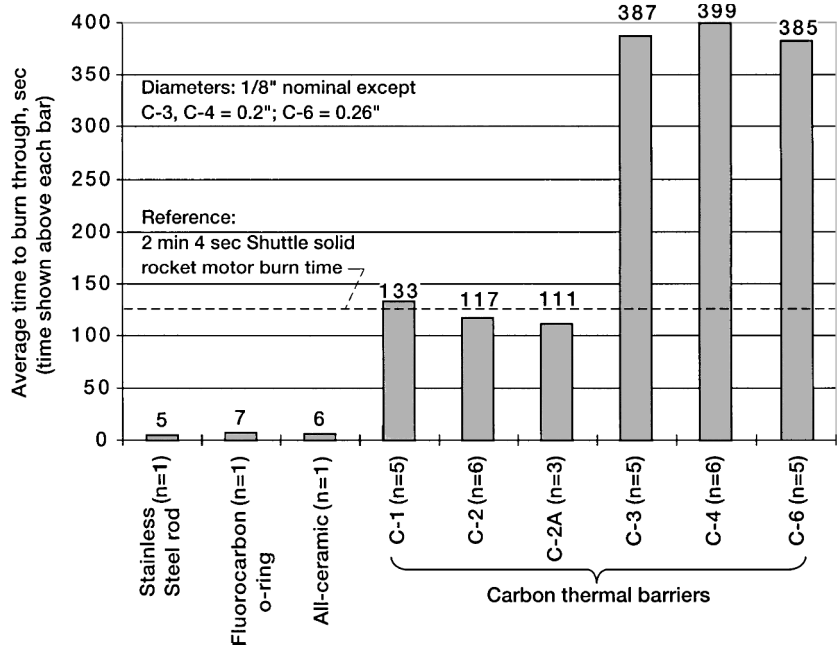

Fig. 5 Oxyacetylene torch burn test results (n = number of tests performed).

were the most burn resistant. Figure 5 summarizes the earlier tests done on $\frac{1}{8}$-in.-diam stainless-steel rods, fluorocarbon O-rings, and all-ceramic braided rope seals. It also shows the burn times of the $\frac{1}{8}$-in.-diam (Carbon-1, Carbon-2, and Carbon-2A) and 0.200-in.-diam (Carbon-3 and Carbon-4) carbon thermal barriers as well as new data on the burn time of the 0.260-in.-diam Carbon-6 design. The $\frac{1}{8}$-in.-diam designs all endured the 5500°F oxyacetylene torch for about 2 min. Even more impressive burn times were seen for the 0.200-in.-diam designs at about 6 $\frac{1}{2}$ min. This is more than three times the shuttle solid-rocket-motor burn time of 2 min, 4 s. However, an increase in diam to 0.260 in. did not produce an increase in burn time. Carbon-6 at 0.260 in. in diameter had a similar burn time to the 0.200-in.-diam designs at about 6 $\frac{1}{2}$ min. Like the other carbon thermal barriers, Carbon-6 was soft and flexible after removal from the flame, even in the area affected by the flame, with no evidence of charring or melting. All of the noncarbon specimens showed signs of charring or melting after removal from the flame, and many became very brittle in the area that was burned.

The similarity in burn time between Carbon-6 and the smaller-diameter Carbon-3 and Carbon-4 thermal barriers is believed to be related to the difference in porosity between these designs. As shown in Table 2, Carbon-6 is more porous than Carbon-3 even in a compressed state. Steinetz and Dunlap[3] theorized that the mass-loss mechanism during the oxyacetylene torch tests was carbon oxidation. Depending on material type, carbon fibers begin to oxidize at temperatures in the range of 600 to 900°F.[7–9] The oxyacetylene torch burning at 5500°F is hot enough to cause oxidation to occur but too cool for carbon sublimation that occurs at 6900°F.[10] It is believed that the looser, more porous braid of Carbon-6 allowed more of the hot, oxidizing torch flame to pass through it. This allowed oxidation to occur more rapidly in the innermost fibers of Carbon-6 than in the less porous Carbon-3 design. Even though there were more carbon fibers in the larger Carbon-6 design, they were cut through more quickly because they were exposed sooner to hot, oxidizing gases. These results indicate that burn/oxidation resistance is dependent on both thermal barrier diameter and porosity.

Products of combustion in the solid rocket motor include liquid alumina (Al_2O_3) and gaseous CO, ClO_2, Cl, HCl, and H_2, none of which are oxidative. Hence, it is believed that the neutral flame in ambient air (oxidizing) is a conservative (i.e., more aggressive) environment for performing material screening burn tests. It is expected that oxidation rates within the rocket environment will be slower than those exhibited herein.

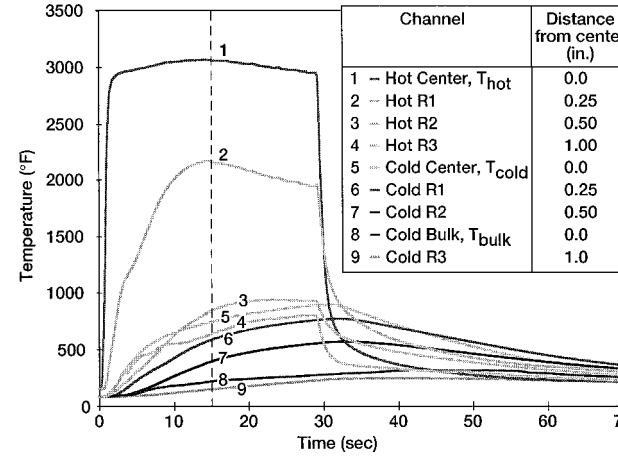

Fig. 6 Temperature rise vs time for simulated hot gas exposure showing upstream (hot) and downstream (cold) temperatures for Carbon-3. Left-hand temperatures removed for clarity.

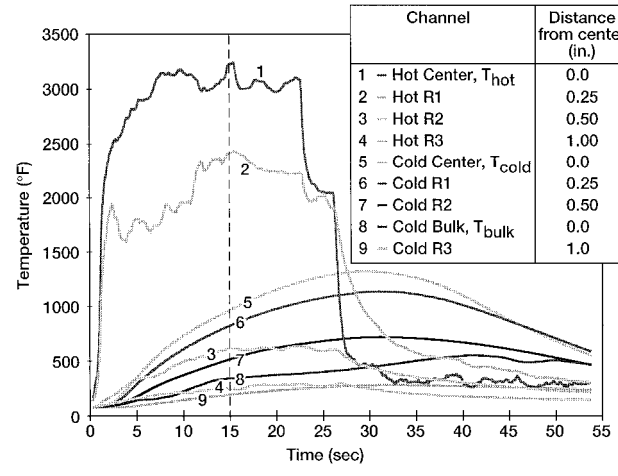

Fig. 7 Temperature rise vs time for simulated hot gas exposure showing upstream (hot) and downstream (cold) temperatures for Carbon-6. Left-hand temperatures removed for clarity.

Temperature Drop Test Results

Temperature drop tests were performed on the Carbon-3 and Carbon-6 thermal barrier designs using the test fixture described that measured the temperature drop across and along the thermal barrier in a compressed state when subjected to the flame of an oxyacetylene torch. Figure 6 shows temperature vs time traces for a test performed on a Carbon-3 specimen. Data recorded from the center thermocouple and the three thermocouples to the right of center on both the hot and cold sides of the specimen are presented. Data from the thermocouples to the left of the center thermocouple are not shown in this figure for clarity. In general, the left and right sides produced symmetric data. Also shown in the figure is the temperature trace from the "cold bulk" (T_{bulk}) thermocouple that measures the air temperature $\frac{1}{4}$ in. downstream of the specimen. For sensitivity purposes the T_{bulk} thermocouple was moved spatially to see if any local "hot streaks" were missed, and none were found. Figure 7 shows temperature traces for a test performed on a Carbon-6 specimen.

Examining Figs. 6 and 7, it can be seen that the center thermocouple on the hot side (T_{hot}) and the center thermocouple on the cold side (T_{cold}) of the thermal barrier each recorded the hottest temperatures on their respective sides. This is expected as these thermocouples are directly in line with the hottest part of the torch flame as it passes through the hole in the iris plate. These figures also show that the temperature got progressively cooler from the center thermocouple to the R1, R2, and R3 thermocouples on the hot and cold sides of the specimen. This was also expected as the temperature decayed with movement further away from the center heat source.

Figures 6 and 7 show that there was a lag between increases in temperature on the hot and cold sides of the specimen. When the torch was applied to the thermal barrier, the hot-side thermocouples instantly registered the increase in temperature. The insulating properties of the thermal barrier delayed heat conduction to the cold side so that the cold-side thermocouples did not register an increase in temperature until several seconds after the torch was applied. The cold-side temperatures measured were significantly lower than the hot-side temperatures, as will be discussed next. After the torch was pulled away from the specimen, the hot-side thermocouples instantly showed a decrease in temperature. The cold-side thermocouples, though, continued to increase for 3 to 5 s before beginning to decrease in temperature. Comparing the hot-side temperatures in Figs. 6 and 7, one notes fluctuations in temperature for Carbon-6 but not Carbon-3. The origin of this fluctuation is unclear at this point, but no system source of the variation was found (e.g., thermocouple integrity, etc.).

Figure 8 shows the temperature drop across specimens of Carbon-3 and Carbon-6 for flame applications of ~30 s. The temperature drop was calculated as the difference between the temperature recorded by the hot-side center thermocouple and the cold-side bulk temperature (T_{bulk}). Over the 30-s torch application, the temperature drop across the Carbon-3 specimen dropped from a high of 2870 to 2680°F by the end of the test. This drop was caused by a steady rise in the cold-side bulk temperature while the hot-side temperature remained nearly constant. Carbon-6 exhibited a temperature drop in the range of 2980 to 2600°F. The uneven nature of the Carbon-6

Table 3a Carbon-3 temperature drop test results

Test number	Exposure time, Per test, s	Exposure time, Accumulated, s	T_{hot} at 15 s, °F	T_{bulk} at 15 s, °F	$T_{hot} - T_{bulk}$ at 15 s, °F	$T_{hot} - T_{cold}$ at 15 s, °F	Flow at 15 s, SCFM/in.	T_{bulk} maximum, °F	Recession after test, in.	Recession after test, %
30	30	30	3070	210	2860	2330	0.14	310	——	——
31	30	60	3050	230	2820	2300	0.14	340	——	——
32	60	120	3020	200	2820	2250	0.14	500	——	——
33	60	180	2590	150	2440	1920	0.14	340	0.029	13

Table 3b Carbon-6 temperature drop test results

Test number	Exposure time, Per test, s	Exposure time, Accumulated, s	T_{hot} at 15 s, °F	T_{bulk} at 15 s, °F	$T_{hot} - T_{bulk}$ at 15 s, °F	$T_{hot} - T_{cold}$ at 15 s, °F	Flow at 15 s, SCFM/in.	T_{bulk} maximum, °F	Recession after test, in.	Recession after test, %
35	30	50	2730	170	2560	2050	0.24	320	——	——
36	30	80	2690	190	2500	1960	0.24	350	——	——
37	60	140	2520	280	2240	1760	0.25	480	——	——
38	60	200	2700	280	2420	1700	0.24	620	0.092	30

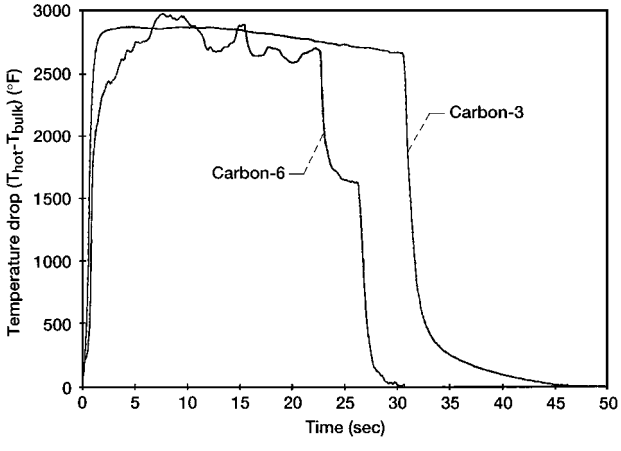

Fig. 8 Temperature drop vs time (T_{hot}–T_{bulk}) at flame location for Carbon-3 and Carbon-6.

trace is caused by fluctuations in the hot-side temperature, as already noted. As shown by these figures, both Carbon-3 and Carbon-6 thermal barrier designs caused a comparable temperature drop across the thermal barrier over a 30-s torch flame application.

Figure 9 illustrates the symmetry of the temperature drop data for Carbon-3 and Carbon-6. Figure 9a shows the temperatures recorded by the seven hot- and cold-side thermocouples that were in contact with the surface of a Carbon-3 specimen 15 s into the test. Though the downstream volume in the nozzle-to-case joint of the shuttle solid rocket motors is expected to fill in less than 10 s, 15 s was chosen to include a safety factor of 5 s. Figure 9b shows similar data for a test performed on Carbon-6. Both figures show the temperature distribution from left to right across the hot and cold sides of the thermal barriers. The center thermocouples on the hot and cold sides correspond to a position of zero. Thermocouples to the left of center have a negative position value, whereas those to the right have a positive value. Both figures show a temperature distribution that is close to symmetric around the center thermocouples. Figure 9a shows that the data for this Carbon-3 test are shifted slightly to the right. Both figures show a temperature drop of about 2300°F between the hot (T_{hot}) and cold (T_{cold}) center thermocouples in contact with the surface of the specimens.

Jet Spreading

The jet spreading capability of Carbon-3 and Carbon-6 is also shown in Fig. 9. Although the hot (3000+°F) torch was focused into a narrow (0.084-in.-diam) column, the thermal barrier spread the heat at least 1 in. on either side of the center thermocouples.

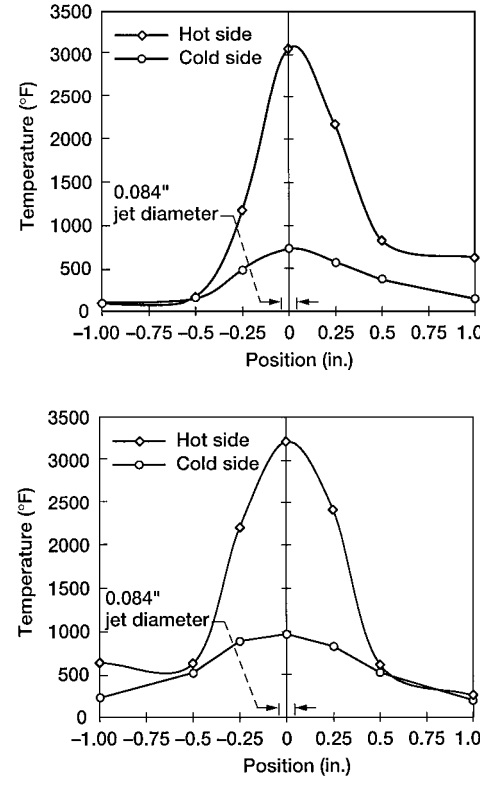

Fig. 9 Hot-side and cold-side temperatures vs axial position at 15 s showing jet (0.084 in. diam) spreading for thermal barriers: a) Carbon-3 and b) Carbon-6.

Figure 9a shows that for Carbon-3 temperatures $\frac{1}{4}$ in. away from the center hot-side thermocouple were about 1200°F on the left side and over 2000°F on the right side. Hot-side data for Carbon-6 in Fig. 9b show a similar trend with temperatures $\frac{1}{4}$ in. away from center over 2200°F. Cold-side data from both Figs. 9a and 9b show that the hot gas jet was reduced in temperature and diffused. Reducing the thermal energy per unit area is beneficial in preventing hot gas effects on the downstream O-rings.

Focused Jet Endurance Tests

Table 3 and Fig. 10 summarize the results of repeated temperature drop tests performed on single specimens of Carbon-3 and Carbon-6 to examine their endurance after multiple applications of the oxy-acetylene torch. For both thermal barrier designs a single specimen

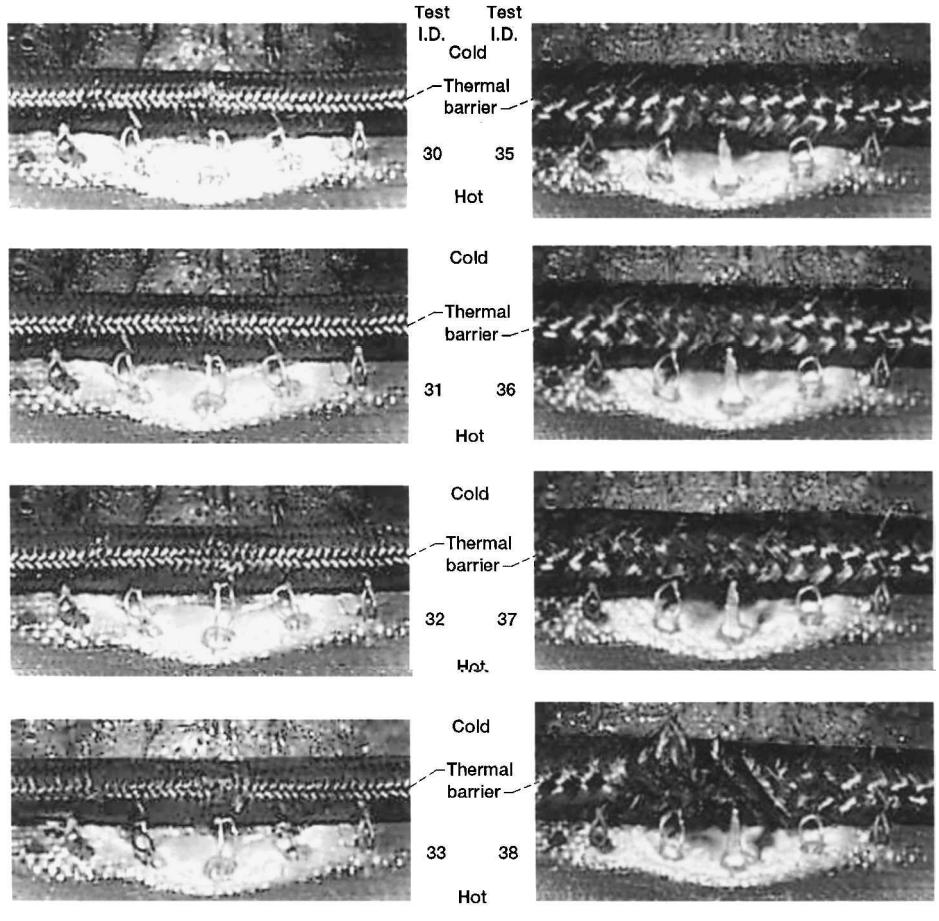

(a) Carbon-3 Temperature Drop Test Results

Test#	Exposure Time		T_{hot}	T_{bulk}	T_{hot}-T_{bulk}
	Per test	Accumulated	@15 sec	@15 sec	@ 15 sec
	(sec)	(sec)	(°F)	(°F)	(°F)
30	30	30	3070	210	2860
31	30	60	3050	230	2820
32	60	120	3020	200	2820
33	60	180	2590	150	2440

(b) Carbon-6 Temperature Drop Test Results

Test#	Exposure Time		T_{hot}	T_{bulk}	T_{hot}-T_{bulk}
	Per test	Accumulated	@15 sec	@15 sec	@ 15 sec
	(sec)	(sec)	(°F)	(°F)	(°F)
35	30	50	2730	170	2560
36	30	80	2690	190	2500
37	60	140	2520	280	2240
38	60	200	2700	280	2420

Fig. 10 Thermal barrier condition and key temperatures vs accumulated time: a) Carbon-3 and b) Carbon-6.

was subjected to the torch flame for two 30-s periods followed by two 60-s periods. The exposure times of 30 and 60 s are longer than the joint cavity fill time of 10 s but were selected to examine the thermal barrier's insulation and flame resistance properties. After each exposure the specimen was photographed (with fixture cover plate removed) to record any specimen damage before the next test was performed. For reference, the Carbon-6 specimen was also exposed to a 20-s flame application before these endurance tests, and no damage was observed.

Table 3 shows several important temperature measurements for each test after 15 s as well as the flow through the specimen at 15 s, the maximum bulk temperature reached during a test, and the amount of recession on the hot side of the specimen after the final flame exposure. The data for Carbon-3 shows that tests 30, 31, and 32 were almost identical. Each showed a maximum hot-side temperature slightly above 3000°F and a temperature drop ($T_{hot}-T_{bulk}$) of over 2800°F. The only difference between these tests was the higher maximum bulk temperature of 500°F in test 32. This was caused by the longer flame exposure time that allowed the bulk temperature to keep increasing for 60 s as compared to the 30-s exposures in tests 30 and 31. The maximum hot-side temperature in test 33 only reached 2590°F compared to 3000+°F in the other tests. This caused lower temperature differences across the specimen and lower bulk temperatures. For all four tests the highest bulk temperature after 15 s was 230°F. This is well below a fluorocarbon O-ring's short-term maximum operating temperature limit of 600°F.[11] Even the maximum bulk temperature of 500°F recorded after 60 s of flame exposure was within the limit. Figure 10a shows the hot side of the Carbon-3 specimen after all four flame exposures. No damage can be seen after the first three tests with little if any damage evident after the final test. As shown in Table 3, there was a recession of 0.029 in. (13% of the compressed cross section) measured after 180 s of exposure. The thermal barrier should never experience such a prolonged exposure to jets of hot gas in the actual rocket application.

The endurance tests performed on Carbon-6 revealed results slightly different than for Carbon-3. After 15 s the maximum temperature ranged from 2520 to 2730°F with temperature drops ($T_{hot}-T_{bulk}$) that ranged from 2240 to 2560°F. The maximum bulk temperature after 15 s was 280°F, slightly higher than that for Carbon-3 but still well below the fluorocarbon O-ring temperature limit. The Carbon-6 series revealed a slightly higher maximum overall bulk temperature of 620°F that occurred in the final test after a 60-s flame exposure. This temperature is about the maximum that the O-rings can withstand for a short period of time, but as already mentioned previously the thermal barrier should not experience such a long flame exposure in the rocket.

Figure 10b shows the hot side of the Carbon-6 specimen after all four flame exposures. Very little damage can be seen after the first test, but the amount of damage to the specimen increased to

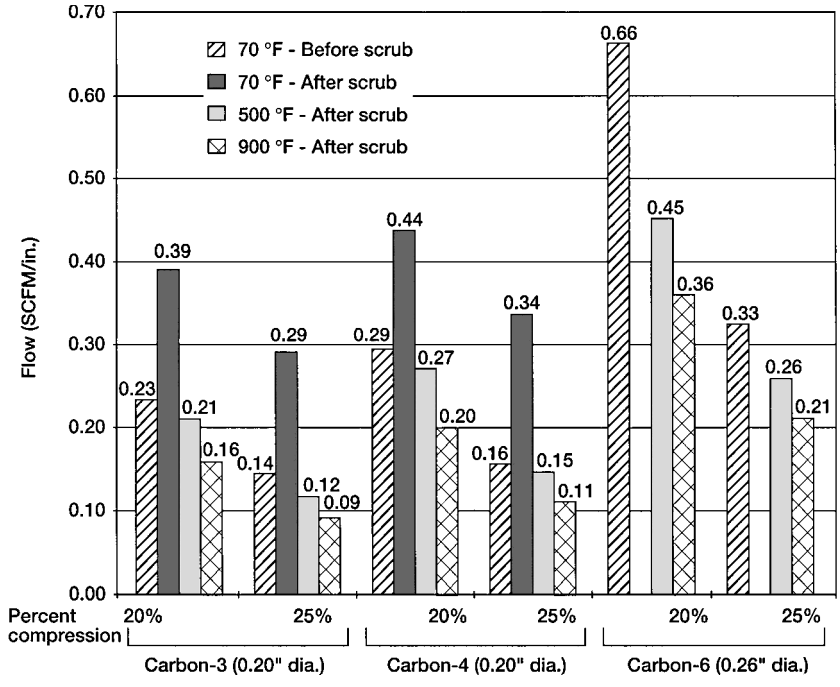

Fig. 11 Effect of temperature, thermal barrier type, scrubbing and compression on flow, $\Delta P = 60$ psid.

a maximum recession of 0.092 in. (30% of the compressed cross section) after the final test. This recession likely contributed to the increased maximum bulk temperature in the final test. These temperature drop tests were all performed in a more aggressive oxidizing environment than the thermal barrier would experience in the rocket. The amount of damage observed on the Carbon-6 specimen after 200 s of flame exposure would not be expected to occur in a less oxidizing environment with much shorter hot gas exposures.

For both series of tests, the flow through the specimen was almost identical from test to test. Flow rates through Carbon-6 were higher than those through Carbon-3 as is expected because Carbon-6 is more porous than Carbon-3 (Table 2).

Flow Test Results

Flow rates (measured using the piston flow rig, Fig. 3) for Carbon-3, Carbon-4, and Carbon-6 at 20 and 25% linear compression are summarized in Fig. 11 at 60 psid and 70, 500, and 900°F after scrubbing and 70°F before scrubbing. Application of the thermal barrier in the shuttle solid-rocket-motornozzle-to-case joint involves predominantly static (e.g., no scrubbing) loads. As shown by the flow results, flow resistance increased with higher compression levels. Figure 11 shows that the flow rates for Carbon-6 were higher than those for Carbon-3 and Carbon-4 at 60 psid at each temperature and compression level. Carbon-6 flow rates were 2.1 to 2.9 times higher than Carbon-3 flow rates and 1.7 to 2.3 times higher than Carbon-4 flow rates at comparable temperatures and compression levels. This difference is caused by differences in braid architecture between these thermal barrier designs. The difference in flow rates between Carbon-3 and Carbon-4 was attributed to Carbon-4 incorporating larger core fibers resulting in higher seal porosity than Carbon-3 (Ref. 3). Carbon-6 incorporating multiple sheath layers has a higher porosity than Carbon-3 (Table 2) and is therefore more permeable. Discussions between the authors and rocket manufacturer Thiokol have indicated that the thermal barriers have high enough permeability to permit the joint cavities to fill in acceptable times.

Effect of Temperature

Figure 11 shows that flow rates dropped for each thermal barrier as the temperature was increased. This phenomenon is explained by the relationship that gas viscosity increases with temperature, $\mu \alpha T^{\frac{2}{3}}$. Thus, as the viscosity of the gas flowing through the thermal barriers increased, the flow rate decreased.[2]

Effect of Hot Scrubbing

Thermal barrier flow rates typically rose after hot scrubbing during flow tests. After 500°F testing Carbon-6 flow rates rose as much as 20% as compared to the flow rates before scrubbing. Postscrub room temperature flows for all thermal barriers were done after time spent at 500°F (2 hr) and 900°F (1.5 hr). Postscrub room temperature flow rates for Carbon-3 as much as doubled as compared to their prescrub values. Carbon-6 exhibited similar flow growth after scrubbing, but flows for pressure differentials of 60 psid were not within the range of the flow meter used. It is believed that much of the flow rate increase is caused by oxidation that occurred while the specimen soaked at these high temperatures. No major visible damage as a result of scrubbing was observed on any of the thermal barrier designs at the conclusion of the flow tests. Only minor fraying was observed at the specimen ends in the lap joint. Temperature exposure tests performed on carbon fiber thermal barriers[3] showed that short lengths of carbon thermal barrier lost weight when heated in a furnace at different temperatures for 2-hour exposures. This supported the theory that the carbon thermal barriers oxidized when exposed to temperatures of 900°F for extended periods of time, and the associated weight loss contributed to the increased flow rates after scrubbing.

Compression Test Results

Table 4 summarizes the results of the compression tests performed on Carbon-3 and Carbon-6 and includes the measured contact width, preload, and residual interference for each amount of linear compression, or crush, tested.

Contact Width

The contact width increased for the Carbon-3 and 6 designs as the amount of linear crush was increased. The thermal barriers continued to spread and flatten out as they experienced larger amounts of compression. In each test the footprint pattern left on the pressure-sensitive film after a compression cycle was solid and continuous. This indicates that during a flow test continuous contact is made between the walls of the flow fixture and the thermal barrier, minimizing leakage past the specimen.

Table 4 Thermal barrier contact width, preload, and residual interference for several linear crush conditions

Thermal barrier type	Diameter, in.	Nominal percent linear crush, %	Linear crush, in.	Number of sheath layers	Contact width, in.	Preload, psi	Residual interference,[a] in.
Carbon-3	0.200	20	0.040	5	0.063	310	0.019
		25	0.050		0.082	490	0.027
		30	0.060		0.099	930	0.033
Carbon-6	0.260	20	0.052	10	0.157	56	0.025
		25	0.065		0.192	80	0.036
		30	0.078		0.196	97	0.041

[a]Residual interference is defined as the distance that the thermal barrier will spring back while maintaining a load of at least 1 lb/in. of specimen.

The contact width at each compression level for Carbon-6 was over twice as large as it was for Carbon-3 even though the diameter of Carbon-6 was only 1.3 times larger than for Carbon-3. This shows that Carbon-6 had a softer, more compressible braid architecture than Carbon-3 allowing Carbon-6 to spread out more as it was compressed.

Preload

The amount of preload or footprint contact pressure increased with the amount of linear crush. However, Carbon-6 had preloads that were $\frac{1}{6}$th to $\frac{1}{9}$th those for Carbon-3 at each compression level. As a result, Carbon-6 will cause lighter loads on the adjoining rubber J-leg element. The reason for this difference in preload is believed to be related to the architectures of these thermal barrier designs (Table 1). In Carbon-3 having a tightly packed core of uniaxial fibers, there is little room for individual fibers to move with respect to one another when they are compressed. In contrast, in Carbon-6 the sheath fibers are oriented at an angle with each other and are better able to slide past each other when the thermal barrier is compressed.

Residual Interference

As with the contact width and preload, thermal barrier residual interference or spring back also increased as percent linear crush increased. Although contact width and preload were quite different for Carbon-6 and Carbon-3, residual interference scaled with diameter for these two designs. Increasing thermal barrier diameter by a factor of 1.3 from 0.200 to 0.260 in. resulted in an increase in residual interference by that ratio for each level of compression. Residual interference for Carbon-6 was 0.025 in. even for the lowest compression (20%) and meets the design requirement to follow nozzle joint movement during shuttle solid-rocket-motor operation, as discussed with rocket manufacturer Thiokol.

Comparison of Carbon-3 and Carbon-6: Other Factors

Carbon-3 and Carbon-6 both performed well in the temperature drop comparison tests. Carbon-3 did offer somewhat greater insulating effects than Carbon-6 and showed less recession than Carbon-6. We believe the higher density of Carbon-3 is an important reason for these results. However, there are other factors to consider when deciding between these two braid architectures. Carbon-6 is braided using larger tows or yarns that permits faster and therefore most cost-effective production. Carbon-6 is also a more flexible braid that makes it easier to spool for shipment and more accommodating during installation.

Results of Thiokol Char Motor Tests on Carbon Thermal Barrier

Thiokol tested a 0.260-in.-diam Carbon-6 thermal barrier for NASA in a subscale rocket motor to verify that it would withstand the shuttle solid-rocket-motor environment. The subscale motor, or char motor, simulates the thermal conditions of the full-scale motor by burning solid rocket propellant at corresponding chamber pressure and temperature conditions. The thermal barrier was placed into an intentional gap defect between the phenolic insulation blocks, as shown in Fig. 12a. The combination of an outboard plenum chamber and the 0.060-in. circumferential gap extending both upstream and downstream of the thermal barrier ensured that hot gas flow would pass through the thermal barrier.

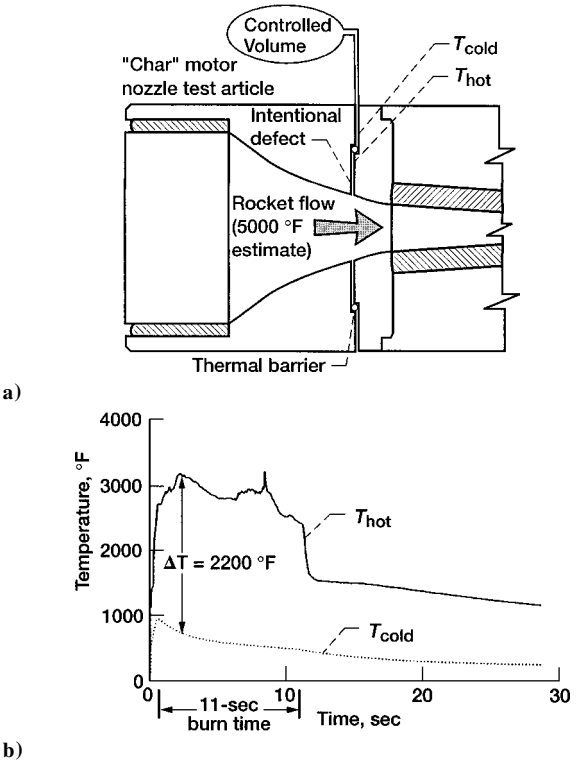

Fig. 12 Subscale (70 lbm) char motor tests examining thermal barrier (Carbon-6) effectiveness: a) test configuration: Carbon-6 thermal barrier impedes hot gas flow through intentional joint defect (0.06 in. gap) and b) temperature data: upstream (T_{hot}) and downstream (T_{cold}) sides of thermal barrier (courtesy of Thiokol Corp.).

Throughout the test duration of ~11 s, a significant drop in temperature was measured across the thermal barrier. Figure 12b shows that the maximum temperature seen on the hot side of the thermal barrier was over 3200°F, while the cold-side temperature reached about 950°F. Thus, a temperature drop of about 2200°F occurred across the 0.260-in.-diam thermal barrier. Pressure readings upstream and downstream of the thermal barrier and in the reservoir confirmed that there was gas flow across the thermal barrier. The thermal barrier diffused the focused nature of the hot gas jet, further reducing the jet's potentially damaging effects on downstream fluorocarbon O-rings in the actual shuttle solid rocket motor.

Although the 950°F temperature recorded downstream of the thermal barrier is still higher than the temperature limits of the fluorocarbon nozzle O-rings, the char motor subjected the thermal barrier to more aggressive conditions than would ever occur in the actual shuttle solid rocket motor for the following reasons. First the gap defect was purposely oversized at 0.060 in. to force flow through the

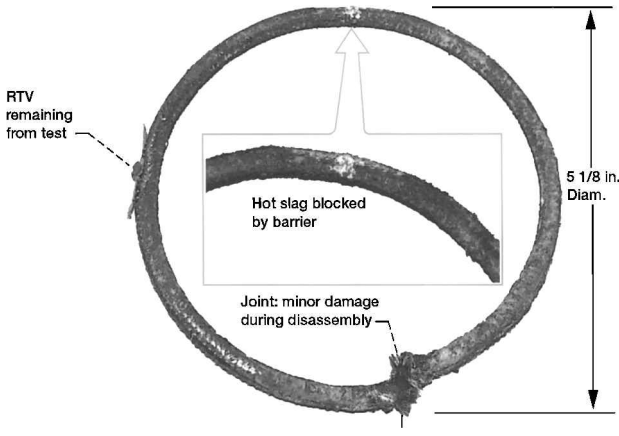

Fig. 13 Photograph of char motor thermal barrier (Carbon-6) after test. Thermal barrier effectively blocks 3200°F gas for 11 s (joint fill time) and blocks hot slag (courtesy of Thiokol Corp.).

thermal barrier. In the actual nozzle joint the gap between adjoining blocks of insulation would be narrower as the pieces of insulation are basically in contact with each other. The narrow gaps between the phenolic insulation would significantly cool the incoming gas temperature impinging on the thermal barrier and would therefore lower the temperature of the gas that reaches the fluorocarbon O-rings. Furthermore, the downstream temperature in the char motor test was recorded immediately downstream of the thermal barrier. The O-rings in the rocket nozzle joint are located several inches further downstream of the thermal barrier, allowing additional heat to be removed from the gas before reaching the O-rings.

Figure 13 shows the thermal barrier after it was removed from the char motor. There was no apparent burning or charring of the thermal barrier. In addition, Fig. 13 shows that the thermal barrier also acted as an effective slag barrier. The inset photo in the figure shows a close-up of an area where slag was trapped by the thermal barrier, preventing it from reaching the downstream O-rings. Minor fraying occurred in the area immediately around the lap joint during disassembly, but the specimen is otherwise in good condition.

The fixture used to perform the temperature drop tests on the Carbon-3 and Carbon-6 thermal barriers was modeled after the char motor and the shuttle nozzle-to-case joint thermal conditions. The fixture was made out of phenolic material to simulate the material and boundary conditions that the thermal barrier would be exposed to in these other configurations. The thermal barrier specimens were subjected to 20% compression as they were in the char motor test and as planned for the rocket. The flame of the oxyacetylene torch that was used for the temperature drop tests was directed through a 0.084-in.-diam hole in an iris plate to simulate a hot gas jet that the barrier could be exposed to in the rocket. Flame exposure times were intentionally longer than they would be in the rocket application to simulate extreme heating conditions.

Considering the results of Fig. 10 (NASA temperature drop fixture), tests were performed with hot-side temperatures ranging from 2500 to nearly 3200°F. Carbon-6 temperature drops ranged from 2240 to 2560°F 15 s into the test. These were somewhat greater than the 2200°F temperature drop exhibited by Carbon-6 in the char motor. The main reason for this difference is that 900-psi pressures were generated by the char motor, whereas only 10-psid pressures were applied across the thermal barrier in the temperature drop tests. The higher-pressure char motor test caused more hot gas to flow through the thermal barrier thereby raising the downstream temperature and causing a smaller temperature drop. Though there are some differences in the absolute results, the authors believe the laboratory temperature drop test fixture simulates many of the key factors at work in the rocket. The laboratory setup permits quick and easy comparisons between competing architectures and can be used to generate thermal data to anchor thermal correlations under development.

Conclusions

The 5500+°F combustion gases in the space-shuttle solid rocket motor are kept a safe distance away from the assembly joint seals by thick layers of insulation and by special compounds that fill the joint split lines in the insulation. The current nozzle-to-case joint design incorporates primary, secondary, and wiper (innermost) O-rings and polysulfide joint-fill compound. In the current design one out of seven motors experiences hot gas to the wiper O-ring. Though the condition does not threaten motor safety, evidence of hot gas to the wiper O-ring results in extensive reviews before resuming flight. NASA and solid-rocket-motor manufacturer Thiokol are examining a redesign of the nozzle-to-case joint in which a more reliable J-leg design (successfully used in the field and igniter joints) and the thermal barrier Carbon-6 described herein are implemented.

The thermal resistance of two NASA thermal barriers, denoted Carbon-3 and Carbon-6, was assessed by exposing them to an oxyacetylene torch at 5500°F and measuring time for burn through. Temperature drop tests were performed to measure the temperature drop across and along the thermal barriers in a compressed state when subjected to the flame of an oxyacetylene torch. Flow and durability tests were conducted on the thermal barriers to examine their leakage characteristics and durability at ambient and high temperatures. Room-temperature compression tests were performed to determine load vs linear compression, preload, contact area, and residual interference/resiliency characteristics. Subscale rocket char motor tests were performed in which hot combustion gases were directed at the Carbon-6 thermal barrier to assess its thermal resistance in a rocket environment. Based on the results of the current tests, the following conclusions are made:

1) The Carbon-6 (0.260-in.-diam) and Carbon-3 (0.20-in.-diam) thermal barriers resisted the 5500°F flame of an oxyacetylene torch for over 6 min before burn through, greater than three times the shuttle solid-rocket-motor burn time.

2) Carbon-3 and Carbon-6 thermal barriers were excellent insulators causing temperature drops through their diameter from 2500 to 2800°F, depending on test parameters. Gas temperatures $\frac{1}{4}$ in. downstream of the thermal barrier were within the downstream fluorocarbon O-ring temperature limit of ≤ 600°F.

3) The Carbon-6 thermal barrier design performed extremely well in subscale rocket char motor tests that subjected it to hot gas at 3200°F for an 11-s rocket firing, simulating the maximum downstream joint-cavity fill time. The thermal barrier reduced the incoming hot gas temperature by 2200°F in an intentionally oversized gap defect, spread the incoming jet flow, and blocked hot slag, thereby offering protection to the downstream O-rings.

4) Laboratory burn, temperature drop, flow, and compression tests and subscale rocket char motor tests demonstrate the thermal barrier's feasibility for use in rocket applications and qualify it for comprehensive motor evaluation.

Acknowledgments

The authors greatly acknowledge Doug Frost's and Steve Hicken's (Thiokol) thermal barrier test results; Bruce Bond's (Albany-Techniweave) assistance in fabricating the thermal barriers; and Tom Doeberling's and Lauren Yee's (NASA) assistance in test support.

References

[1] Steinetz, B. M., Adams, M. L., Bartolotta, P. A., Darolia, R., and Olsen, A., "High Temperature Braided Rope Seals for Static Sealing Applications," *Journal of Propulsion and Power*, Vol. 13, No. 5, 1997, pp. 675–682.

[2] Steinetz, B. M., and Adams, M. L., "Effects of Compression, Staging, and Braid Angle on Braided Rope Seal Performance," *Journal of Propulsion and Power*, Vol. 14, No. 6, 1998, pp. 934–940.

[3] Steinetz, B. M., and Dunlap, P. H., "Feasibility Assessment of Thermal Barriers for Extreme Transient Temperatures," *Journal of Propulsion and Power*, Vol. 16, No. 2, 2000, pp. 347–356.

[4] Stein, S. R., "RSRM-45A Nozzle Joint No. 3 O-Ring Erosion Investigation Team—Final Report," Thiokol Corporation, TWR-73191, Brigham City, UT, Oct. 1996.

[5] Rogers, W. P., "Report of the Presidential Commission on the Space

Shuttle Challenger Accident," Govt. Printing Office, Washington, DC, June 1986.

[6]Ballis, W., *ASM Handbook, Volume 6: Welding, Brazing, and Soldering*, ASM International, Materials Park, OH, 1993, pp. 281–290.

[7]Bahl, O. P., and Dhami, T. L., "Oxidation Resistance of Carbon Fibers," *High Temperatures—High Pressures*, Vol. 19, No. 2, 1987, pp. 211–214.

[8]Eckstein, B. H., and Barr, J. B., "An Accelerated Oxidation Test for Oxidation Resistant Carbon Fibers," *Materials-Processes: The Intercept Point; Proceedings of the Twentieth International SAMPE Technical Conference*, Society for the Advancement of Materials and Process Engineering, Covina, CA, 1988, pp. 379–391.

[9]Eckstein, B. H., "The Weight Loss of Carbon Fibers in Circulating Air," *Proceedings of the Eighteenth International SAMPE Technical Conference*, Society for the Advancement of Materials and Process Engineering, Covina, CA, 1986, pp. 149–160.

[10]Lide, D. R., and Kehiaian, H. V., *CRC Handbook of Thermophysical and Thermochemical Data*, CRC Press, Boca Raton, FL, 1994, pp. 25–31.

[11]Parker Seal Group, *Parker O-Ring Handbook*, Parker Hannifin Corporation, Lexington, KY, 1992, p. A3,A4.